Supporting Information: Chemistry in Quantum Cavities: Exact Results, the Impact of Thermal Velocities and Modified Dissociation

Dominik Sidler,[*,†] Michael Ruggenthaler,[*,†] Heiko Appel,[*,†] and Angel Rubio[*,†,‡,¶]

†*Max Planck Institute for the Structure and Dynamics of Matter and Center for Free-Electron Laser Science & Department of Physics, Luruper Chaussee 149, 22761 Hamburg, Germany*

‡*Center for Computational Quantum Physics, Flatiron Institute, 162 5th Avenue, New York, NY 10010, USA*

¶*Nano-Bio Spectroscopy Group, Universidad del Pais Vasco, 20018 San Sebastian, Spain*

E-mail: dsidler@mpsd.mpg.de; michael.ruggenthaler@mpsd.mpg.de; heiko.appel@mpsd.mpg.de; angel.rubio@mpsd.mpg.de

1 Theoretical Details

1.1 Center of Mass (COM) Separation

In order to tackle the coupled light-matter problem defined by the Pauli-Fierz Hamiltoninan, given in Eq. (1) of the letter, in dipole approximation, it is useful to switch to a centre-of-mass (COM) coordinate system. This means that we define $\mathbf{r}_i = \mathbf{R}_c + \mathbf{r}_{ci}$, with the COM explicitly given as $\mathbf{R}_c := \frac{\sum_i m_i \mathbf{r}_i}{\sum_i m_i}$. The Hamiltonian can then be re-written in the COM frame as,

$$\hat{H} = \frac{\hat{\mathbf{P}}_c^2}{2M} + \sum_{i=1}^{N} \frac{\hat{\mathbf{p}}_{ci}^2}{2m_i} + \sum_{i<j}^{N} \frac{Z_i Z_j}{|\hat{\mathbf{r}}_{ci} - \hat{\mathbf{r}}_{cj}|} + \sum_{\alpha=1}^{M} \frac{1}{2}\left[\hat{p}_\alpha^2 + \omega_\alpha^2 \Big(\hat{q}_\alpha - \frac{\boldsymbol{\lambda}_\alpha}{\omega_\alpha} \cdot \hat{\mathbf{R}}\Big)^2\right]. \tag{S1}$$

Note that *a priori* the dipole operator still contains a COM dependence at this stage. In a next step, we apply the unitary Power-Zienau-Woolley (PZW) transformation shifting the COM,

$$\hat{U}_{PZW} := e^{i \frac{Q_{\text{tot}} \boldsymbol{\lambda}_\alpha \cdot \hat{\mathbf{R}}_c}{\omega_\alpha} \hat{p}_\alpha}, \tag{S2}$$

with $Q_{\text{tot}} := \sum_{i=1}^{N} eZ_i$. By using the Baker-Campbell-Hausdorf formula, one can show that our PZW transformation obeys the following properties,

$$\hat{U}_{PZW} \hat{p}_\alpha \hat{U}_{PZW}^\dagger = \hat{p}_\alpha \tag{S3}$$

$$\hat{U}_{PZW} \hat{q}_\alpha \hat{U}_{PZW}^\dagger = \hat{q}_\alpha + i \frac{Q_{\text{tot}} \boldsymbol{\lambda}_\alpha \cdot \hat{\mathbf{R}}_c [\hat{p}_\alpha, \hat{q}_\alpha]}{\omega_\alpha} \tag{S4}$$

$$\hat{U}_{PZW} \hat{\mathbf{R}}_c \hat{U}_{PZW}^\dagger = \hat{\mathbf{R}}_c \tag{S5}$$

$$\hat{U}_{PZW} \hat{\mathbf{P}}_c \hat{U}_{PZW}^\dagger = \hat{\mathbf{P}}_c + i \frac{Q_{\text{tot}} \boldsymbol{\lambda}_\alpha \cdot [\hat{\mathbf{R}}_c, \hat{\mathbf{P}}_c]}{\omega_\alpha} \hat{p}_\alpha, \tag{S6}$$

which allow to write the shifted Hamiltonian as,

$$\hat{H}' = \frac{1}{2M}\left(\hat{\mathbf{P}}_c - \sum_{\alpha=1}^{M}\frac{\lambda_\alpha Q_{\rm tot}}{\omega_\alpha}\hat{p}_\alpha\right)^2 + \sum_{i=1}^{N}\frac{\hat{\mathbf{p}}_{ci}^2}{2m_i} + \sum_{i<j}^{N}\frac{Z_i Z_j}{|\hat{\mathbf{r}}_{ci}-\hat{\mathbf{r}}_{cj}|} \tag{S7}$$

$$+\sum_{\alpha=1}^{M}\frac{1}{2}\left[\hat{p}_\alpha^2 + \omega_\alpha^2\left(\hat{q}_\alpha - \frac{\boldsymbol{\lambda}_\alpha}{\omega_\alpha}\cdot\sum_{i=1}^{N}Z_i\hat{\mathbf{r}}_{ci}\right)^2\right], \tag{S8}$$

by applying the PZW transformation for each mode α. Afterwards, the original eigenvalue problem $H\psi = E\psi$ can be simplified to Eq. (2) given in the letter by using a wave function Ansatz of the form $\psi'(R_c, r_c, q_\alpha) = e^{i\mathbf{k}\boldsymbol{R}_c}\Phi'(r_c, q_\alpha)$. For one mode α and three bodies, one obtains the following expression,

$$\left[\frac{1}{2M}\left\{\mathbf{k}^2 + \frac{2Q_{\rm tot}\mathbf{k}\cdot\boldsymbol{\lambda}}{\omega'}\hat{p}'\right\} + \sum_{i=1}^{3}\frac{\hat{\mathbf{p}}_{ci}^2}{2m_i} + \sum_{i<j}^{3}\frac{Z_i Z_j}{|\hat{\mathbf{r}}_{ci}-\hat{\mathbf{r}}_{cj}|}\right.$$

$$\left. +\frac{1}{2}\left[\hat{p}'^2 + \omega'^2\left(\hat{q}' - \frac{\boldsymbol{\lambda}}{\omega'}\cdot\sum_{i=1}^{3}Z_i\hat{\mathbf{r}}_{ci}\right)^2\right]\right] e^{i\mathbf{k}\boldsymbol{R}_c}\Phi' = Ee^{i\mathbf{k}\boldsymbol{R}_c}\Phi'. \tag{S9}$$

In case of neutral systems (i.e. $Q_{\rm tot} = 0$), the additional interaction of the COM motion with the quantized field vanishes. Note that in Eq. (S9) it was used that for one mode (i.e. $M = 1$) the PZW-shifted eigenvalue problem can be additionally simplified by absorbing $\frac{1}{M}\left(\frac{\lambda Q_{\rm tot}}{\omega}\right)^2$ in a dressed resonance frequency, $\omega' = \omega\sqrt{1 + \frac{1}{M}\left(\frac{\lambda Q_{\rm tot}}{\omega}\right)^2}$ with the corresponding momenta $\hat{p}' = i\sqrt{\frac{\omega'}{2}}(\hat{a}^\dagger - \hat{a})$ and position operators $\hat{q}' = \sqrt{\frac{1}{2\omega'}}(\hat{a}^\dagger + \hat{a})$. They obey the usual canonical commutation relations $[\hat{q}', \hat{p}'] = i$. This shift will only be relevant for relatively light charged particles at low resonance frequencies ω (e.g. fundamental L0-L1 transition of HD+).

1.2 Observables

When calculating observables of the coupled system ($\lambda \neq 0$), *a priori* one cannot neglect any involved coordinate. However, in practise not always all integrals have to be solved explicitly. For example, the dipole oscillatory strengths can be calculated from COM relative

coordinates $\mathbf{r}_{ci}$ as follows:

$$\begin{aligned}\mathrm{Osc}_{jk} &= \frac{2}{\frac{1}{m_1}+\frac{1}{m_2}+\frac{1}{m_3}}(E_j-E_k)|\langle\psi_j|\,\hat{\mathbf{R}}\otimes\mathbb{1}_{pt}\,|\psi_k\rangle \\ &= \frac{2}{\frac{1}{m_1}+\frac{1}{m_2}+\frac{1}{m_3}}(E_j-E_k)|\langle\psi'_j|\sum_{i=1}^{3}Z_i e\hat{\mathbf{r}}_{ci}\otimes\mathbb{1}_{pt}\,|\psi'_k\rangle\,, \end{aligned} \tag{S10}$$

where in the last step it was used that $\langle\psi|\,\hat{\mathbf{R}}\otimes\mathbb{1}_{pt}\,|\psi\rangle = \langle\psi'|\,\hat{U}_{PZW}(\hat{\mathbf{R}}\otimes\mathbb{1}_{pt})\hat{U}^{\dagger}_{PZW}\,|\psi'\rangle = \langle\psi'|\,\hat{\mathbf{R}}\otimes\mathbb{1}_{pt}\,|\psi'\rangle$ with Eq. (S5).

In contrast, photonic observables have to be transformed back to the length gauge to be consistent. Hence, an integration over the COM position has to be performed explicitly. However, due to the cylindrically symmetric setup with respect to the z-axis of the lab frame, i.e.

$$\langle\psi|\,\mathbb{1}_{\mathrm{matter}}\otimes\hat{O}_{pt}\,|\psi\rangle = \langle\psi'|\,\mathbb{1}_{\mathrm{matter}}\otimes\hat{U}(Z_c)\hat{O}_{pt}\hat{U}^{\dagger}_{PZW}(Z_c)\,|\psi'\rangle\,, \tag{S11}$$

the COM integration is reduced to one dimension only.

The general expectation-value integral in our chosen spherical-cylindrical coordinate system (see Sec. 1.3 below) is given as,

$$\begin{aligned}\langle\psi|\,\hat{O}\,|\psi\rangle &= \langle\psi'|\,\hat{U}_{PZW}\hat{O}(p_{ci},r_{ci},\hat{p},\hat{q})\hat{U}^{\dagger}_{PZW}\,|\psi'\rangle \\ &= \sum_{n=0}^{\infty}\int_{-\infty}^{\infty}dR_{cx}\int_{-\infty}^{\infty}dR_{cy}\int_{-\infty}^{\infty}dR_{cz}\int_{-\infty}^{\infty}d\zeta\int_{0}^{\infty}dR\int_{0}^{\infty}d\rho\int_{0}^{2\pi}d\phi\int_{0}^{\pi}d\theta\int_{0}^{\pi}d\psi \\ &\quad R^2\rho\sin\theta e^{-ik_zR_{cz}}\Phi'^{*}e^{i\frac{Q_{\mathrm{tot}}\lambda R_{cz}\hat{p}}{\omega}}\hat{O}e^{-i\frac{Q_{\mathrm{tot}}\lambda R_{cz}\hat{p}}{\omega}}e^{ik_zR_{cz}}\Phi' \qquad \text{(S12)} \\ &= \sum_{n=0}^{\infty}\int_{-\infty}^{\infty}dR_{cz}\int_{-\infty}^{\infty}d\zeta\int_{0}^{\infty}dR\int_{0}^{\infty}d\rho\int_{0}^{2\pi}d\phi\int_{0}^{\pi}d\theta\int_{0}^{\pi}d\psi \qquad \text{(S13)} \\ &\quad R^2\rho\sin\theta\Phi'^{*}e^{i\frac{Q_{\mathrm{tot}}\lambda R_{cz}\hat{p}}{\omega}}\hat{O}e^{-i\frac{Q_{\mathrm{tot}}\lambda R_{cz}\hat{p}}{\omega}}\Phi', \qquad \text{(S14)}\end{aligned}$$

where in the last step it was assumed that $\hat{O}$ does not explicitly depend on the COM coordinate and positions. Note, if $\lambda = 0$ or if $Q_{\mathrm{tot}} = 0$ or if $\hat{O}$ does not depend on $\hat{q}$ and P_{cz},

the R_{cz} integral is unity as it was the case for a matter only system.

1.3 Numerical Implementation

1.3.1 Spatial Coordinate Representation

In order to make an exact solution of a quantized three-body system coupled to one cavity mode feasible, a smart choice of the spatial representation of the matter is pivotal. For this purpose we follow the approach in Refs. 1,2, which is known to reach excellent numerical accuracy for matter only calculations of three bodies, with only moderate computational costs. This means, we represent the COM relative coordinates $\mathbf{r}_{ci}$ of our three bodies in a 6-dimensional combined spherical and cylindrical coordinate system. Its angular coordinates $\{\theta, \phi, \psi\}$ will eventually be treated analytically, whereas the radial coordinates $\{R, \rho, \zeta\}$ will be treated numerically after an additional transformation into perimetric coordinates.

To obtain the combined spherical and cylindrical coordinates, one expresses the COM relative coordinates $\mathbf{r}_{ci}$ in terms of two vectors $\mathbf{X},\ \mathbf{Y}$, which are chosen such that $\mathbf{r}_{c2}-\mathbf{r}_{c1} = \mathbf{X}$, $\mathbf{r}_{c1} - \mathbf{r}_{c3} = \mathbf{X} + \frac{\mathbf{Y}}{2}$ and $\mathbf{r}_{c2} - \mathbf{r}_{c3} = \mathbf{X} - \frac{\mathbf{Y}}{2}$. Moving the origin of $\mathbf{X},\ \mathbf{Y}$ to the COM, results in,

$$\mathbf{r}_{c1} = \frac{m_2 + \frac{m_3}{2}}{M}\mathbf{X} + \frac{m_3}{M}\mathbf{Y} \tag{S15}$$

$$\mathbf{r}_{c2} = -\frac{m_1 + \frac{m_3}{2}}{M}\mathbf{X} + \frac{m_3}{M}\mathbf{Y} \tag{S16}$$

$$\mathbf{r}_{c3} = \frac{m_2 - m_1}{2M}\mathbf{X} - \frac{m_1 + m_2}{M}\mathbf{Y}. \tag{S17}$$

In a next step, one expresses $\mathbf{X}$ in spherical coordinates and $\mathbf{Y}$ in cylindrical coordinates

with respect to $\mathbf{X}$. The resulting expressions are,[2]

$$\mathbf{X} = \begin{bmatrix} R\sin\theta\cos\phi \\ R\sin\theta\sin\phi \\ R\cos\theta \end{bmatrix} \tag{S18}$$

$$\mathbf{Y} = \begin{bmatrix} (\rho\cos\theta\cos\psi + \zeta\sin\theta)\cos\phi - \rho\sin\psi\sin\phi \\ (\rho\cos\theta\cos\psi + \zeta\sin\theta)\sin\phi + \rho\sin\psi\cos\phi \\ -\rho\sin\theta\cos\psi + \zeta\cos\theta. \end{bmatrix} \tag{S19}$$

Using Eqs. (S15)-(S17), the COM relative coordinates $\mathbf{r}_{ci}(R,\theta,\phi,\rho,\psi,\zeta)$ with $\zeta \in [-\infty,\infty[$,$\{R,\rho\} \in [0,\infty[$, $\{\phi,\psi\} \in [0,2\pi[$ and $\theta \in [0,\pi[$ can be expressed in the combined coordinate system, which are explicitly given as[2,3]

$$\mathbf{r}_{c1} = \begin{bmatrix} x_{c1} \\ y_{c1} \\ z_{c1} \end{bmatrix} = \begin{bmatrix} \frac{m_2+m_3/2}{M} R\sin\theta\cos\phi + \frac{m_3}{M}\big((\rho\cos\theta\cos\psi + \zeta\sin\theta)\cos\phi - \rho\sin\psi\sin\phi\big) \\ \frac{m_2+m_3/2}{M} R\sin\theta\sin\phi + \frac{m_3}{M}\big((\rho\cos\theta\cos\psi + \zeta\sin\theta)\sin\phi - \rho\sin\psi\cos\phi\big) \\ \frac{m_2+m_3/2}{M} R\cos\theta + \frac{m_3}{M}\big(-\rho\sin\theta\cos\psi + \zeta\cos\big) \end{bmatrix} \tag{S20}$$

$$\mathbf{r}_{c2} = \begin{bmatrix} x_{c2} \\ y_{c2} \\ z_{c2} \end{bmatrix} = \begin{bmatrix} -\frac{m_1+m_3/2}{M} R\sin\theta\cos\phi + \frac{m_3}{M}\big((\rho\cos\theta\cos\psi + \zeta\sin\theta)\cos\phi - \rho\sin\psi\sin\phi\big) \\ -\frac{m_1+m_3/2}{M} R\sin\theta\sin\phi + \frac{m_3}{M}\big((\rho\cos\theta\cos\psi + \zeta\sin\theta)\sin\phi - \rho\sin\psi\cos\phi\big) \\ -\frac{m_1+m_3/2}{M} R\cos\theta + \frac{m_3}{M}\big(-\rho\sin\theta\cos\psi + \zeta\cos\big) \end{bmatrix} \tag{S21}$$

$$\mathbf{r}_{c3} = \begin{bmatrix} x_{c3} \\ y_{c3} \\ z_{c3} \end{bmatrix} = \begin{bmatrix} \frac{m_2-m_1}{2M} R\sin\theta\cos\phi - \frac{m_1+m_2}{M}\big((\rho\cos\theta\cos\psi + \zeta\sin\theta)\cos\phi - \rho\sin\psi\sin\phi\big) \\ \frac{m_2-m_1}{2M} R\sin\theta\sin\phi - \frac{m_1+m2}{M}\big((\rho\cos\theta\cos\psi + \zeta\sin\theta)\sin\phi - \rho\sin\psi\cos\phi\big) \\ \frac{m_2-m_1}{2M} R\cos\theta - \frac{m_1+m_2}{M}\big(-\rho\sin\theta\cos\psi + \zeta\cos\big) \end{bmatrix}, \tag{S22}$$

and the corresponding transformed volume element becomes

$$dV = R^2\rho\sin(\theta) dR_{cx} dR_{cy} dR_{cz} d\zeta dR d\rho d\phi d\theta d\psi. \tag{S23}$$

A sketch of the combined coordinate system is given in Fig. S1.

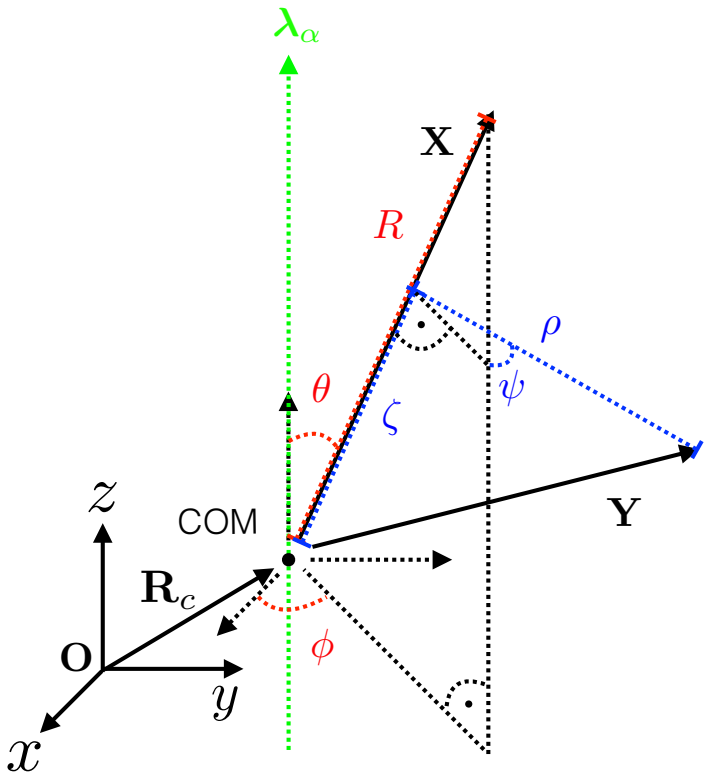

Figure S1: Schematics of the coordinate system. We assume the relevant (green) cavity mode polarized along the z-direction, i.e. $\boldsymbol{\lambda}_\alpha \parallel \mathbf{z}$. The spherical coordinates of vector $\mathbf{X}$ are shown in red, whereas the cylindrical coordinates of vector $\mathbf{Y}$ are displayed in blue.

1.3.2 Basis Set Expansion

First of all, λ-coupling is assumed along the z-axis only, i.e.

$$\boldsymbol{\lambda}_\alpha = \begin{bmatrix} 0 \\ 0 \\ \lambda_\alpha \end{bmatrix}. \tag{S24}$$

In a next step, we employ the Ansatz wave function defined in Eq. (3) of the main text, which gives access to the formally exact solution for $N_l, N_m, N_{pt} \rightarrow \infty$. For uncoupled setups (i.e. $\lambda = 0$), l refers to the to the angular quantum number and m to the magnetic quantum number, which describe the total angular momentum relation $L^2 = l(l+1)$ and its z-projection $L_z = m$. Suppose we want to restrict the magnetic quantum number m to zero, which is a priori a reasonable choice for a matter only or uncoupled systems by setting $N_m = 0$.

Due to the choice of $\boldsymbol{\lambda} \parallel z$, i.e. by preserving the cylindrical symmetry with respect to the z-axis of the lab frame, and by using the definition of Wigner D-Matrices $D^j_{m,k} = e^{-im\phi} d^j_{m,k}(\theta) e^{-ik\psi}$ with Wigner's (small) d-matrix defined according to standard literature, one can show that $\langle \Phi_{l',m'} | H'_{pt} | \Phi_{l,m} \rangle = \delta_{m',m} \langle \Phi_{l',m'} | H'_{pt} | \Phi_{l,m} \rangle$, since H'_{pt} does not depend on ϕ. In other words, restricting $m = 0$ is a valid choice even for coupled systems. However, the coupling of the photons to the matter starts to mix angular states. Hence, one cannot diagonalize the coupled Hamiltonian anymore for each angular momentum quantum number l separately, which increases the dimensionality of the coupled problem considerably apart from the extra photonic degree of freedom. For practical reasons (implementation amount and computational load), we restrict the basis size to S and P states only, i.e. $l < 2$, for all subsequent calculations. Therefore, the Wigner-D matrix wave function Ansatz, given in Eq. (3) of the main text, can be rewritten in terms of superpositions of even (e) and odd

(o) wave-functions of the P-states leading to the following orthonormal basis[3]

$$\Phi'_S := \frac{1}{\sqrt{8\pi}}\varphi_S(R,\rho,\zeta)\otimes|n\rangle \tag{S25}$$

$$\Phi'_P{}^{\mathrm{e}} := \frac{\sqrt{3}}{\sqrt{8\pi}}\sin(\theta)\cos(\psi)\varphi^{\mathrm{e}}_P(R,\rho,\zeta)\otimes|n\rangle \tag{S26}$$

$$\Phi'_{P0}{}^{\mathrm{o}} := \frac{\sqrt{3}}{\sqrt{8\pi}}\cos(\theta)\varphi^{\mathrm{o}}_{P0}(R,\rho,\zeta)\otimes|n\rangle \tag{S27}$$

$$\Phi'_{P1}{}^{\mathrm{o}} := -\frac{\sqrt{3}}{\sqrt{8\pi}}\sin(\theta)\cos(\psi)\varphi^{\mathrm{o}}_{P1}(R,\rho,\zeta)\otimes|n\rangle\,. \tag{S28}$$

The resulting representation of the Pauli-Fierz Hamiltonian takes the following block-diagonal form:

$$\begin{aligned}\mathscr{H}' &= \mathscr{H}'_m+\mathscr{H}'_{pt} = \begin{bmatrix} H_{SS}(\hat{\mathbf{p}}_{ci},\hat{\mathbf{r}}_{ci}) & 0 & 0 & 0\\ 0 & H_{PP}(\hat{\mathbf{p}}_{ci},\hat{\mathbf{r}}_{ci}) & 0 & 0\\ 0 & 0 & H_{P0P0}(\hat{\mathbf{p}}_{ci},\hat{\mathbf{r}}_{ci}) & H_{P0P1}(\hat{\mathbf{p}}_{ci},\hat{\mathbf{r}}_{ci})\\ 0 & 0 & H_{P1P0}(\hat{\mathbf{p}}_{ci},\hat{\mathbf{r}}_{ci}) & H_{P1P1}(\hat{\mathbf{p}}_{ci},\hat{\mathbf{r}}_{ci})\end{bmatrix}\\ &+\begin{bmatrix} H_{SS}(\hat{\mathbf{r}}_{ci},\hat{p}',\hat{q}') & 0 & H_{SP0}(\hat{\mathbf{r}}_{ci},\hat{q}') & H_{SP1}(\hat{\mathbf{r}}_{ci},\hat{q}')\\ 0 & H_{PP}(\hat{\mathbf{r}}_{ci},\hat{p}',\hat{q}') & 0 & 0\\ H_{P0S}(\hat{\mathbf{r}}_{ci},\hat{q}') & 0 & H_{P0P0}(\hat{\mathbf{r}}_{ci},\hat{p}',\hat{q}') & H_{P0P1}(\hat{\mathbf{r}}_{ci},\hat{q}')\\ H_{P1S}(\hat{\mathbf{r}}_{ci},\hat{q}') & 0 & H_{P1P0}(\hat{\mathbf{r}}_{ci},\hat{q}') & H_{P1P1}(\hat{\mathbf{r}}_{ci},\hat{p}',\hat{q}')\end{bmatrix}\end{aligned} \tag{S29}$$

where the first term corresponds to the matter-only problem promoted to the coupled matter-photon space, e.g. $H_{ij} = H^m_{ij}\otimes\mathbb{1}_{\mathrm{pt}}$ with matrix elements H^m_{ij} given in the literature.[2] Note that vanishing matrix entries in the first term are due to parity symmetry of the uncoupled problem. Vanishing matrix entries in the second term are obtained by analytical angular integration in combination with the chosen basis set truncation at $l = 1$. The matrix elements are explicitly given as

$$H_{SP0,ij} = H_{P0S,ji} = -\frac{\sqrt{3}}{3}\omega\lambda\Bigg\langle\Bigg\{Z_1\Big[\frac{m_1+m_3/2}{M}R+\frac{m_3}{M}\zeta\Big] \tag{S30}$$
$$+Z_2\Big[-\frac{m_1+m_3/2}{M}R+\frac{m_3}{M}\zeta\Big]+Z_3\Big[\frac{m_2-m_1}{2M}R-\frac{m_1+m_2}{M}\zeta\Big]\Bigg\}\hat{q}'\Bigg\rangle_{ij}$$

$$H_{SP1,ij} = H_{P1S,ji} = \frac{\sqrt{3}}{3}\omega\lambda\Bigg\langle\Bigg\{-Z_1\frac{m_3}{M}-Z_2\frac{m_3}{M}+Z_3\frac{m_1+m_2}{M}\Bigg\}\rho\hat{q}'\Bigg\rangle_{ij} \tag{S31}$$

$$H_{SS,ij} = \Bigg\langle\frac{1}{2}\Bigg\{\frac{k_z^2}{M}+\hat{p}'^2+\omega'^2\hat{q}'^2+\frac{2Q_{\rm tot}k_z\lambda}{M\omega'}\hat{p}'\Bigg\}\Bigg\rangle_{ij}+ \tag{S32}$$
$$\frac{\lambda^2}{2}\Big\langle Z_1^2z_{1c}^2+Z_2z_{2c}^2+Z_3z_{3c}^2+2(Z_1Z_2z_{1c}z_{2c}+Z_1Z_3z_{1c}z_{3c}+Z_2Z_3z_{2c}z_{3c})\Big\rangle_{ij}$$

$$H_{PP,ij} = \Bigg\langle\frac{1}{2}\Bigg\{\frac{k_z^2}{M}+\hat{p}'^2+\omega'^2\hat{q}'^2+\frac{2Q_{\rm tot}k_z\lambda}{M\omega'}\hat{p}'\Bigg\}\Bigg\rangle_{ij}+ \tag{S33}$$
$$\frac{\lambda^2}{2}\Big\langle Z_1^2z_{1c}^2+Z_2z_{2c}^2+Z_3z_{3c}^2+2(Z_1Z_2z_{1c}z_{2c}+Z_1Z_3z_{1c}z_{3c}+Z_2Z_3z_{2c}z_{3c})\Big\rangle_{ij}$$

$$H_{P0P0,ij} = \Bigg\langle\frac{1}{2}\Bigg\{\frac{k_z^2}{M}+\hat{p}'^2+\omega'^2\hat{q}'^2+\frac{2Q_{\rm tot}k_z\lambda}{M\omega'}\hat{p}'\Bigg\}\Bigg\rangle_{ij}+ \tag{S34}$$
$$\frac{\lambda^2}{2}\Big\langle Z_1^2z_{1c}^2+Z_2z_{2c}^2+Z_3z_{3c}^2+2(Z_1Z_2z_{1c}z_{2c}+Z_1Z_3z_{1c}z_{3c}+Z_2Z_3z_{2c}z_{3c})\Big\rangle_{ij}$$

$$H_{P1P1,ij} = \Bigg\langle\frac{1}{2}\Bigg\{\frac{k_z^2}{M}+\hat{p}'^2+\omega'^2\hat{q}'^2+\frac{2Q_{\rm tot}k_z\lambda}{M\omega'}\hat{p}'\Bigg\}\Bigg\rangle_{ij}+ \tag{S35}$$
$$\frac{\lambda^2}{2}\Big\langle Z_1^2z_{1c}^2+Z_2z_{2c}^2+Z_3z_{3c}^2+2(Z_1Z_2z_{1c}z_{2c}+Z_1Z_3z_{1c}z_{3c}+Z_2Z_3z_{2c}z_{3c})\Big\rangle_{ij}$$

$$H_{P1P0,ij} = H_{P0P1,ji} = \frac{\lambda^2}{2}\Big\langle Z_1^2z_{1c}^2+Z_2z_{2c}^2+Z_3z_{3c}^2+ \tag{S36}$$
$$2(Z_1Z_2z_{1c}z_{2c}+Z_1Z_3z_{1c}z_{3c}+Z_2Z_3z_{2c}z_{3c})\Big\rangle_{ij}$$

with

$$z_{1c}^2 = \left(\frac{m_2+m_3/2}{M}\right)^2\beta + \frac{m_3(m_2+m_3/2)}{M^2}\gamma + \left(\frac{m_3}{M}\right)^2\epsilon \tag{S37}$$

$$z_{2c}^2 = \left(\frac{m_1+m_3/2}{M}\right)^2\beta - \frac{m_3(m_1+m_3/2)}{M^2}\gamma + \left(\frac{m_3}{M}\right)^2\epsilon 2 \tag{S38}$$

$$z_{3c}^2 = \left(\frac{m_2-m_1}{2M}\right)^2\beta - \frac{(m_2-m_1)(m_1+m_2)}{2M^2}\gamma + \left(\frac{m_1+m_2}{M}\right)^2\epsilon \tag{S39}$$

$$z_{1c}z_{2c} = -\frac{m_2+m_3/2}{M}\frac{m_1+m_3/2}{M}\beta + \left(\frac{m_2+m_3/2}{M} - \frac{m_1+m_3/2}{M}\right)\frac{m_3}{M}\gamma + \left(\frac{m_3}{M}\right)^2\epsilon \tag{S40}$$

$$z_{1c}z_{3c} = \frac{m_2+m_3/2}{M}\frac{m_2-m_1}{2M}\beta + \left(-\frac{m_2+m_3/2}{M}\frac{m_1+m_2}{M} + \frac{m_3(m_2-m_1)}{2M^2}\right)\gamma - \frac{m_3(m_1+m_2)}{M^2}\epsilon \tag{S41}$$

$$z_{2c}z_{3c} = -\frac{m_1+m_3/2}{M}\frac{m_2-m_1}{2M}\beta + \left(\frac{m_1+m_3/2}{M}\frac{m_1+m_2}{M} + \frac{m_3(m_2-m_1)}{2M^2}\right)\gamma - \frac{m_3(m_1+m_2)}{M^2}\epsilon, \tag{S42}$$

where β, γ, ϵ are defined in spherical-cylindrical coordinates as,

$$\beta = b_1R^2 \tag{S43}$$

$$\gamma = c_1R\zeta - c_2R\rho \tag{S44}$$

$$\epsilon = e_1\rho^2 + e_2\zeta^2 - 2e_3\rho\zeta. \tag{S45}$$

The coefficients contain the analytical evaluation of the angular integrals of the λ^2-term,

which amount to the following non-zero values,

$$b_{1SS} = \frac{1}{3},\ b_{1PP} = b_{1P1P1} = \frac{3}{15},\ b_{1P0P0} = \frac{3}{5} \tag{S46}$$

$$c_{1SS} = \frac{1}{3},\ c_{1PP} = c_{1P1P1} = \frac{3}{15},\ c_{1P0P0} = \frac{3}{5} \tag{S47}$$

$$c_{P0P1} = -\frac{3}{15},\ c_{P1P0} = -\frac{3}{15} \tag{S48}$$

$$e_{1SS} = \frac{1}{3},\ e_{1PP} = e_{1P0P0} = \frac{3}{15},\ e_{1P1P1} = \frac{3}{5} \tag{S49}$$

$$e_{2SS} = \frac{1}{3},\ e_{2PP} = e_{2P1P1} = \frac{3}{15},\ e_{2P0P0} = \frac{3}{5} \tag{S50}$$

$$e_{3P0P1} = -\frac{3}{15},\ e_{3P1P0} = -\frac{3}{15}. \tag{S51}$$

For the λ angular integrals, the resulting $\pm\frac{\sqrt{3}}{3}$ was already included in H_{SP0} and H_{SP1}, respectively. Analysing the matrix given in Eq. (S29) in terms of S, $\mathrm{P_{even}}$ and $\mathrm{P_{odd}}$, one notices that the block-diagonal nature of the non-interacting terms remains preserved by the λ^2-term, only broken by mixing of S and $\mathrm{P_{odd}}$ states due to the λ-term. Note that one can show that S-states do not mix via the λ-term for any excited angular momentum states beyond $l = 1$. However, this is not necessarily true for λ^2 contributions.

1.3.3 Gauss-Laguerre Quadrature for Radial Integrals

So far it was only stated that there is a matrix representation of the coupled Hamiltonian, but it was not yet specified how to treat the radial coordinates $R,\ \zeta,\ \phi$ numerically. For this purpose, a coordinate transformation into a h_i-scaled perimetric coordinate system of the following form is performed in a first step, where

$$\zeta = \frac{(x-y)(x+y+2z)}{4(x+y)} \tag{S52}$$

$$R = \frac{x+y}{2} \tag{S53}$$

$$\rho = \frac{\sqrt{xyz(x+y+z)}}{x+y} \tag{S54}$$

with new volume element [2]

$$dV = h_1 h_2 h_3 \sin(\theta)(\tilde{x}+\tilde{y})(\tilde{x}+\tilde{z})(\tilde{y}+\tilde{z}) dR_{cx} dR_{cy} dR_{cz} d\tilde{x} d\tilde{y} d\tilde{z} d\phi d\theta d\psi, \tag{S55}$$

and $\tilde{x} := h_1 x$, $\tilde{y} := h_2 y$, $\tilde{z} := h_3 z$. The scaling factors h_i will later be used to adjust the radial grid to the spatial extend of simulated syste. In a next step, the orthonormal basis given in Eqs. (S25)-(S28) is rewritten as,

$$\varphi_S(R,\rho,\zeta) = \sum_{i=1}^{N_{\text{matter}}} \sum_{j=1}^{N_{\text{matter}}} \sum_{k=1}^{N_{\text{matter}}} N_{Sijk} F_{ijk}(\tilde{x},\tilde{y},\tilde{z}) \tag{S56}$$

$$\varphi_P^{\text{e}}(R,\rho,\zeta) = \mathscr{R}(\tilde{x},\tilde{y},\tilde{z}) \sum_{i=1}^{N_{\text{matter}}} \sum_{j=1}^{N_{\text{matter}}} \sum_{k=1}^{N_{\text{matter}}} N_{Pijk} \mathscr{R}^{-1}(h_1 x_i, h_2 y_j, h_3 z_j)^{-1} F_{ijk}(\tilde{x},\tilde{y},\tilde{z}) \tag{S57}$$

$$\varphi_{P0}^{\text{o}}(R,\rho,\zeta) = \sum_{i=1}^{N_{\text{matter}}} \sum_{j=1}^{N_{\text{matter}}} \sum_{k=1}^{N_{\text{matter}}} N_{P0ijk} F_{ijk}(\tilde{x},\tilde{y},\tilde{z}) \tag{S58}$$

$$\varphi_{P1}^{\text{o}}(R,\rho,\zeta) = \mathscr{R}(\tilde{x},\tilde{y},\tilde{z}) \sum_{i=1}^{N_{\text{matter}}} \sum_{j=1}^{N_{\text{matter}}} \sum_{k=1}^{N_{\text{matter}}} N_{P1ijk} \mathscr{R}^{-1}(h_1 x_i, h_2 y_j, h_3 z_j) F_{ijk}(\tilde{x},\tilde{y},\tilde{z}), \tag{S59}$$

where a regularization factor $\mathscr{R}(x,y,z) = \rho R = \frac{\sqrt{xyz(x+y+z)}}{2}$ was introduced in agreement with the literature.[3] It suppresses singularities of the matter-only Hamiltonian, which may cause numerical difficulties. However, its only practical relevance is restricted to radial momentum operators, which do not appear in the coupling Hamiltonian and thus $\mathscr{R}$ eventually cancels. The newly introduced scaled Lagrange function $F_{ijk}(\tilde{x},\tilde{y},\tilde{z})$ is defined as,

$$F_{ijk}(\tilde{x},\tilde{y},\tilde{z}) = (N_{ijk} h_1 h_2 h_3)^{-1/2} \tilde{f}_i(\tilde{x}/h_1) \tilde{f}_j(\tilde{y}/h_2) \tilde{f}_k(\tilde{z}/h_2), \tag{S60}$$

with

$$N_{ijk} = (h_1 x_i + h_2 y_j)(h_1 x_i + h_3 z_k)(h_2 y_j + h_3 z_k). \tag{S61}$$

The Lagrange-Laguerre functions are defined as,

$$\tilde{f}_i(u) := (-1)^i u_i^{1/2} \frac{L_{N_{\text{matter}}}(u)}{u - u_i} e^{-u/2} \tag{S62}$$

with L_N the Laguerre polynomial of degree N with roots u_i and Lagrange property $f_i(u_j) = (\lambda_i^N)^{-1/2}\delta_{ij}$. The coefficients λ_i^N can be chosen to fulfill the Gauss-Laguerre quadrature approximation

$$\int_0^\infty G(u)du \approx \sum_{i=1}^N \lambda_i^N G(u_i) = \sum_{i=1}^N h\lambda_i^N G(u_i h). \tag{S63}$$

Notice that for the formation of singlet or triplet states, the matter-only wave functions in Eqs. (S56)-(S59) can be (anti)-symmetrized by proper permutation of the perimetric coordinates (see Ref. 3). Eventually, the matrix elements given in Eqs. (S31)-(S37) assume a simple form,

$$\begin{aligned}
H_{SS} &= \delta_{ii'}\delta_{jj'}\delta_{kk'} H_{SS}(h_1 x_i, h_2 y_j, h_3 z_k) && \text{(S64)}\\
H_{PP} &= \delta_{ii'}\delta_{jj'}\delta_{kk'} H_{PP}(h_1 x_i, h_2 y_j, h_3 z_k) && \text{(S65)}\\
H_{P0P0} &= \delta_{ii'}\delta_{jj'}\delta_{kk'} H_{P0P0}(h_1 x_i, h_2 y_j, h_3 z_k) && \text{(S66)}\\
H_{P1P0} &= H_{P0P1} = \delta_{ii'}\delta_{jj'}\delta_{kk'} H_{P1P0}(h_1 x_i, h_2 y_j, h_3 z_k) && \text{(S67)}\\
H_{P1P1} &= H_{PP} = \delta_{ii'}\delta_{jj'}\delta_{kk'} H_{P1P1}(h_1 x_i, h_2 y_j, h_3 z_k) && \text{(S68)}\\
H_{SP0} &= H_{P0S} = \delta_{ii'}\delta_{jj'}\delta_{kk'} H_{SP0}(h_1 x_i, h_2 y_j, h_3 z_k) && \text{(S69)}\\
H_{SP1} &= H_{P1S} = \delta_{ii'}\delta_{jj'}\delta_{kk'} H_{SP1}(h_1 x_i, h_2 y_j, h_3 z_k), && \text{(S70)}
\end{aligned}$$

by using the orthonormality property of F_{ijk} for the perimetric volume element in Gauss-approximation[3]

$$\int_0^\infty d\tilde{x} \int_0^\infty d\tilde{y} \int_0^\infty d\tilde{z} h_1 h_2 h_3 (\tilde{x}+\tilde{y})(\tilde{x}+\tilde{z})(\tilde{y}+\tilde{z}) F_{ijk}(\tilde{x},\tilde{y},\tilde{z}) F_{i'j'k'}(\tilde{x},\tilde{y},\tilde{z}) = \delta_{ii'}\delta_{jj'}\delta_{kk'} \tag{S71}$$

$N_{ijk} = 1$ is implied from the normalisation condition. Hence, the original eigenvalue problem given in Eq. (S9) is now discretized and numerically accessible by solving

$$\mathscr{H}'\mathbf{c}' = E\mathbf{c}', \tag{S72}$$

for E and $\mathbf{c}$.

2 Simulation Details

2.1 Input Parameters

For all He and HD+ simulations, the following basis set size was chosen: $N_{pt} = 6$, $N_l = 1$, $N_m = 0$, $N_{\text{matter}} = 12$. For H_2^+ the matter grid was slightly increased and combined with a reduce photon number: $N_{pt} = 5$, $N_l = 1$, $N_m = 0$, $N_{\text{matter}} = 16$. Therefore, for each input parameter combination a Hamiltonian matrix of size 41472^2 for distinguishable particles (HD+), 21600^2 for He and 42240^2 for H_2^+ had to be diagonalized. The eigenvalue problem was implemented in the in-house LIBQED python code and the high-performance ELPA library[4] was used for the exact numerical diagonalization.

The particle masses were set according to literature,[3,5] i.e. He: $m_1 = 1$, $m_2 = 1$, $m_3 = 7294.2618241$, HD+: $m_1 = 1836.142701$, $m_2 = 3670.581$, $m_3 = 1$ and H_2^+: $m_1 = 1836.142701$, $m_2 = 1836.142701$, $m_3 = 1$. Corresponding scaling values for the radial Lagrange-Laguerre grid were set to the following values, which were motivated by matter-only considerations in the literature:[2] He: $h_1 = 0.8$, $h_2 = 0.8$, $h_3 = 0.4$, HD+: $h_1 = 0.16$, $h_2 = 0.16$, $h_3 = 1.4$ and H_2^+: $h_1 = 0.33$, $h_2 = 0.33$, $h_3 = 2.0$. The different scaling values account for the difference in the spatial localisation of the constituents and thus allow to reach high numerical accuracy with a relatively coarse radial grid.

2.2 Convergence and Numerical Tests

Multiple explicit convergence/ sanity checks were perform to ensure that finite basis set errors or implementation mistakes do not spoil the results. Matter-only energy eigenvalues were compared with reference calculations from literature given in Tab. S1. For He, the λ^2-scaling of the ground-state could be compared with QEDFT calculations with photon OEP accuracy in the Born-Oppenheimer limit, which indicates an agreement on the same accuracy level as one expects from the previous matter-only considerations (see Fig. S1). All QEDFT simulations were performed with the OCTOPUS code.[6] Note that highly accurate simulations of ground-state nuclear contributions in QEDFT would be very challenging to obtain.[7]

Last but not least, the Thomas-Reiche-Kuhn sum rule was well preserved for He, HD+ and H_2^+, which implies that there is no fundamental implementation error present. Moreover, all observables were consistent with theory and particularly in agreement with the JC model. This offers an additional sanity check of the numerical results (see main section of the manuscript).

Table S1: Despite having a substantially smaller radial matter grid available for our coupled simulations compared with matter-only reference data, our grid allows to reach millihartree accuracies for the absolute energy eigenvalues and orders of magnitude smaller values for corresponding energy-differences. (*) Notice that the $2P^{(odd)}$ state for H_2^+ corresponds to the dissociation limit.[2] In other words, there are no dipole allowed bound state transitions for H_2^+ and a continuum of allowed transitions arises beyond this energy value.

Lowest matter-only energy eigenvalues [H]		
He	Reference[1,3]	$N_{\text{matter}} = 12$
$1S^{(even)}$	-2.9033045555597	-2.90330437154
$2S^{(even)}$	-2.145678586051	-2.14567817793
$2P^{(odd)}$	-2.1235456525895	-2.12320490110
HD+	Reference[8]	$N_{\text{matter}} = 12$
$1S^{(even)}$	-0.59789796860903	-0.59757212
$2P^{(odd)}$	-0.59769812819221	-0.59737196
$2S^{(even)}$	-0.58918182955696	-0.58702708
H_2^+	Reference[2]	$N_{\text{matter}} = 16$
$1S^{(even)}$	-0.597139063121	-0.596973
$2S^{(even)}$	-0.58715567914	-0.585948
$2P^{(odd)*}$	-0.4990065652928^*	-0.498039^*

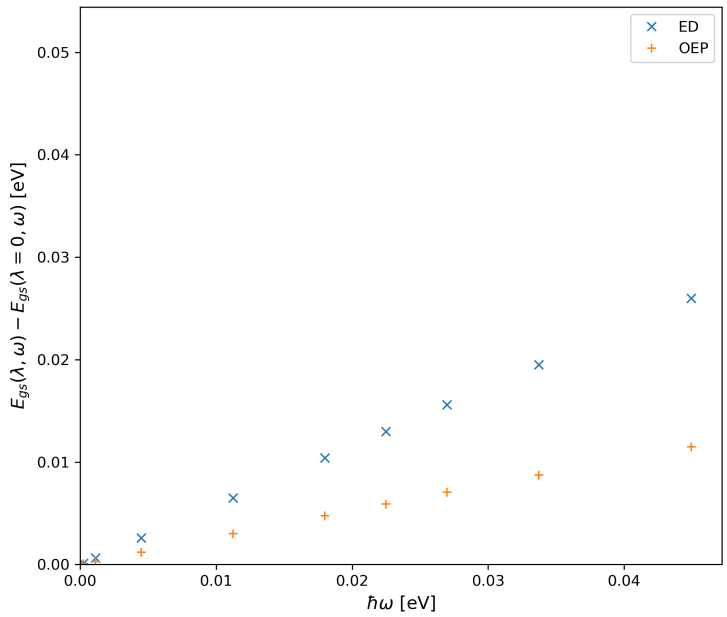

Figure S2: Cutting the basis set expansion for angular momentum quantum numbers $l > 1$, may introduce significant numerical errors for stronger couplings. In order to check the validity by allowing e.g. $l = 2$, the code complexity of the implementation would be more than doubled. Therefore, we decided to use an alternative route. The comparison of the the He ground-state energy shift with results from QEDFT simulations with photon OEP [9] indicates that inaccuracies from $l < 2$, are on the order of milihartree or below, which is in line with the accuracy reached for the absolute matter-only energies given in Tab. S1. As it is the case for matter-only values, one expects considerable smaller relative errors in terms of energy differences.

3 Results: Additional Observables

3.1 He

Figs. S3a - S3b show the parahelium dispersion curves with respect to the mode occupation $\langle \hat{n} \rangle = \langle \hat{a}^\dagger \hat{a} \rangle$ and wave-function overlap between the exact solution and the JC model. Notice, that the ΔE-values in the last figure are obtained from the JC model (i.e. based on matter-only considerations) and not from the exact diagonalisation of the coupled system. The mode occupation (a) clearly highlights the one- to five-photon lines (replica) that appear in our simulations (we have chosen $N_{pt} = 6$ in these simulations). With each further Fock-basis

state in our simulation we would get a further photon line. In (b) we see that for the standard upper and lower polaritons the JC model is highly accurate even on the wave-function level, while the higher photon-replicas are not well captured at resonance.

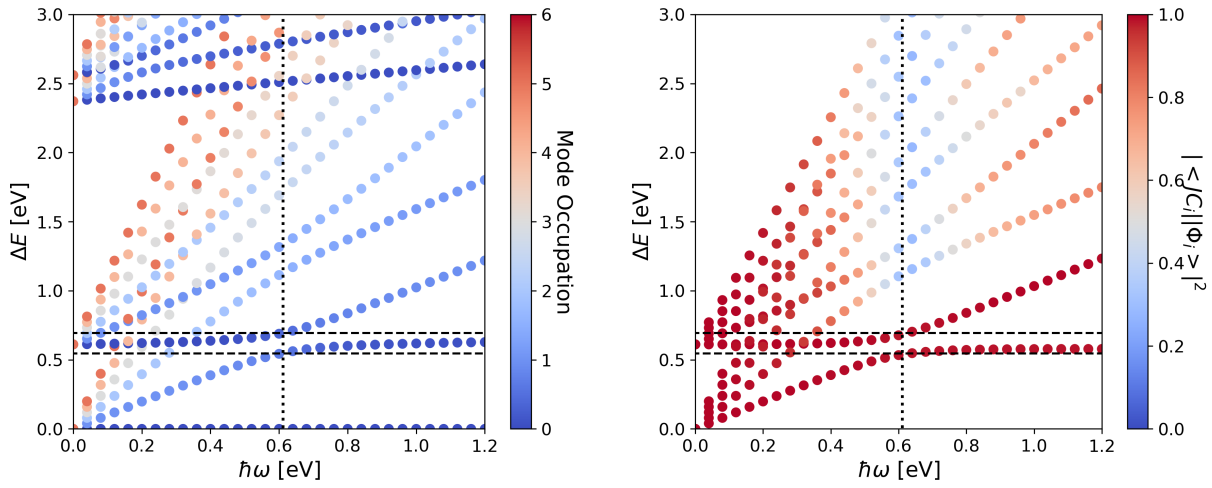

(a) (b)

Figure S3: Parahelium polaritonic dispersion curves in a cavity. The vertical line indicates the 2S-2P resonance where $\lambda = 0.057$ was set. Horizontal lines indicate the splitting of the lowest two polaritons. Notice that $\frac{\sqrt{\omega}}{\lambda}$ was kept fix, i.e. the coupling strength $g \propto \omega\hbar$. In (a) the color bar indicates the photonic observable $\langle \hat{n} \rangle$, whereas in (b) the wave-function overlap between our exact calculation and the corresponding JC model is shown.

3.2 HD+

In Fig. S4 a zoom of the dispersion relations given in the main section is shown to visualize dressing effects, caused by dipole self-interaction, and the shift of the resonance frequency due to the non-zero net-charge. In Fig. S5a the impact of different finite COM velocities on the oscillator strength is shown at resonance condition. The break-down of the JC model at finite COM velocities for charged systems is visualised in Figs. S5b and S5c. They indicate that the relatively high agreement between exact and JC wave function for bright states at $k_z = 0$ breaks down at finite velocities. For such systems one expects for any observable, which is calculated from JC states, to be error-prone at finite COM velocities.

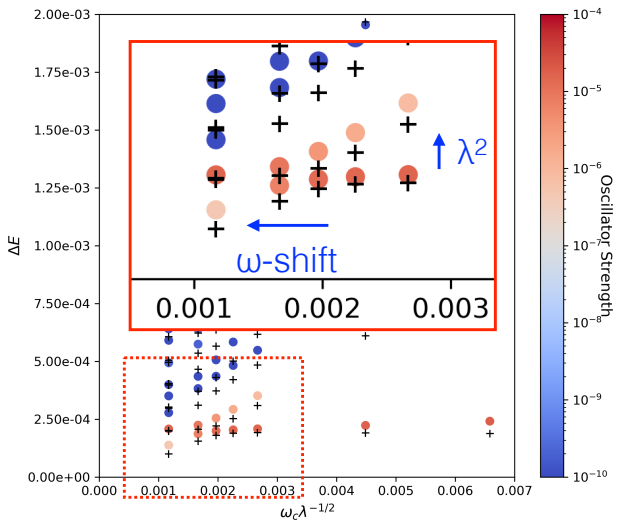

Figure S4: Visualization of the dressed polaritonic dispersion relation of HD+ in a cavity with a frequency centered around the fundamental ro-vibrational transition in atomic units. The shifts are caused by dipole self-interaction contributions (ΔE-shift) and COM influence for non-zero net-charge $\hbar\omega$-shift.

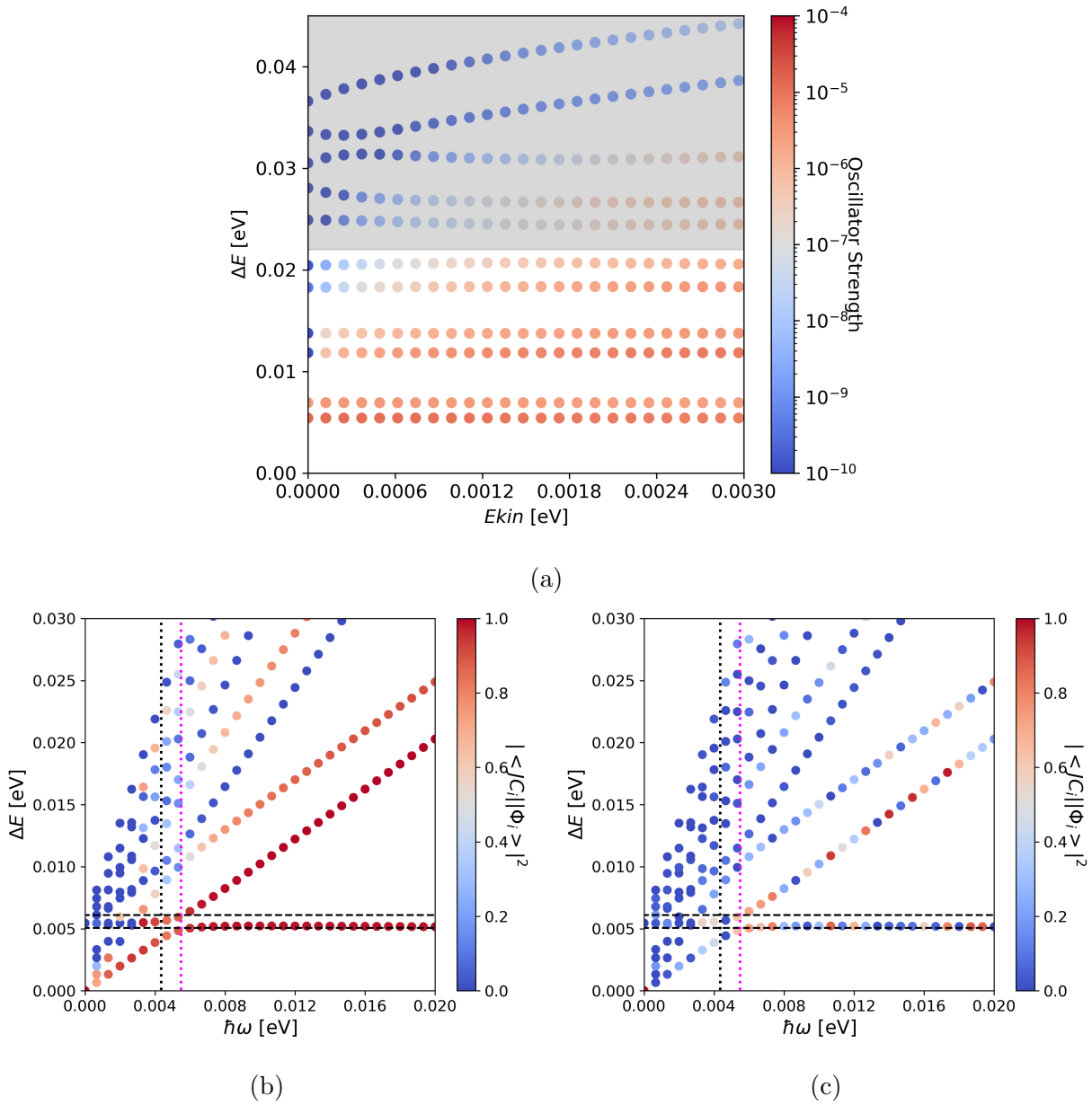

Figure S5: In (a) we consider the HD+ resonant case for ΔE at $\lambda = 0.01$ with respect to the kinetic energy E_{kin} of the COM. While the spectrum is not changed (up to numerical inaccuracies for higher-lying states) the COM motion (a) redistributes the oscillator strengths. Notice that the grey area indicates less reliable eigenvalues, which are not converged for the chosen photon number basis with $N_{pt} = 6$. In (b) and (c) the HD+ polaritonic dispersion curves for $k_z = 0$ and $k_z = 1$ are shown with respect to the wave-function overlap between our exact calculations and the corresponding JC model. The black vertical line indicates the 2S-2P resonance condition $\hbar\omega$ and the purple vertical line indicates the corresponding frequency predicted by the JC model that is missing the frequency dressing. Notice that the energy eigenvalues shown in (b) and (c) are determined by the JC model and not by the exact diagonalisation of the coupled problem. Horizontal lines indicate the splitting of the lowest two polaritons.

3.3 H_2^+

Similarly to HD+, we performed simulations for H_2^+ at different COM velocities (see Figs. S6a - S6b). In contrast to HD+, the frequencies are scanned around the 1S-2P transition, which corresponds to the dissociation limit $H_2^+ \rightarrow H + p$. This adds additional complexity to the interpretation of the computed dispersion relations. One needs to consider that a continuum of dipole-allowed transitions emerges beyond the dissociation limit. However, this cannot be represented on our finite radial grid, which is scaled to reproduce bound-state properties optimally. For this reason, one observes a discrete spectrum of dipole allowed (red) energy levels beyond the dissociation limit. However, there are two ways to identify truly discrete (i.e. bound) peaks in our discretized continuum. First, one can calculate the proton-proton distances for each excited state to identify potentially bound states (see main section). Second, bound excitations are invariant with respect to changes of the radial basis set and the corresponding scaling parameters, whereas the discrete continuum reacts very sensitively. Based on these considerations, we could distinguish the bound states, which are shown in the main section, from continuum states composed of a H-atom and a free proton coupled to the cavity. With the latter method one can also identify the dissociation energy limits, i.e. when increasing the scaling factors of the radial grids one observes an accumulation of eigenvalues at the dissociation energies,[2] while the newly discovered bound polaritonic states remain invariant. Similarly to the main section, in Fig. S7 the proton-proton distance vs. energy plot is shown for the previously identified bound states. However, for this figure we assumed an infinite mass for the nuclei. Qualitatively, the system behaves very similar compared with the results for finite proton masses. Overall, the proton-proton distances of the bound states are slightly reduced and some of the excitation energy differences are moderately shifted compared with the finite mass reference. Nevertheless, the appearance of bound states below and above the dissociation limit remains preserved in the infinite-mass limit.

Aside from that, one can also investigate the bound 1S-iS transitions below the dissoci-

ation limit with respect to different COM velocities. Our simulations for H_2^+ confirm that a finite COM motion of a charged molecule indeed leads to an increased dipole-transition probability, as it was discussed for HD+ in the main section.

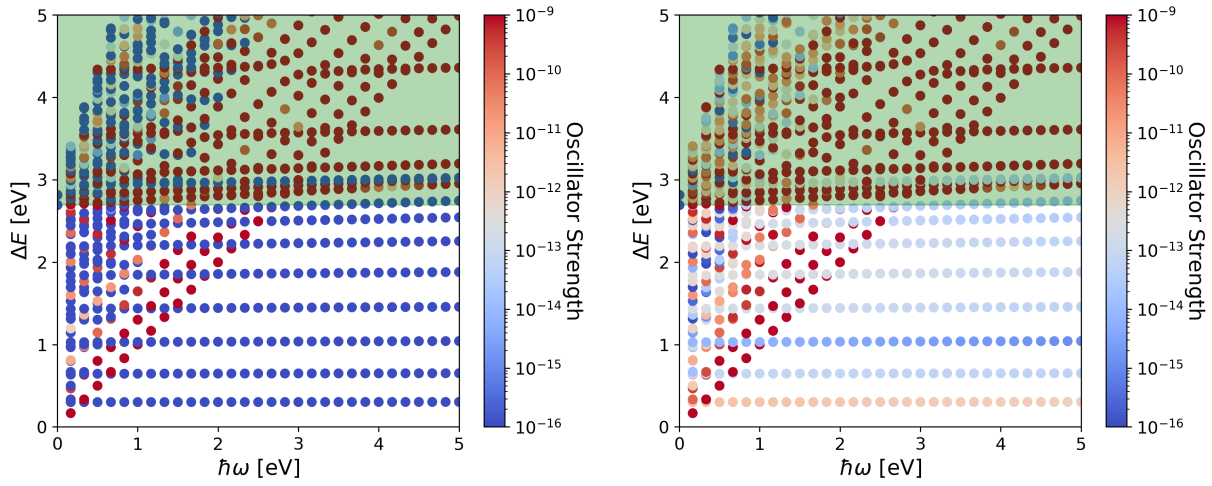

Figure S6: Dispersion relations for the H_2^+ molecule with singlet nuclear spin configuration in a cavity. The frequencies are centered around the dissociation energy of the bare matter system. It is assumed that $\frac{\sqrt{\hbar\omega}}{\lambda} = const$, i.e. the coupling strength $\propto \omega$, and $\lambda = 0.057$ at resonance with the dissociation energy. The oscillator strength color bar is chosen to visualize changes arising from finite COM velocities in a relatively weak regime. The COM motion was set to $E_{kin} = 0$ for (a), whereas for (b) a non-vanishing $E_{kin} = 0.37$ [eV] was chosen, which is still in the non-relativistic limit, i.e. $k \approx 0.072c$. The vertical dotted line indicates the dissociation resonance condition.

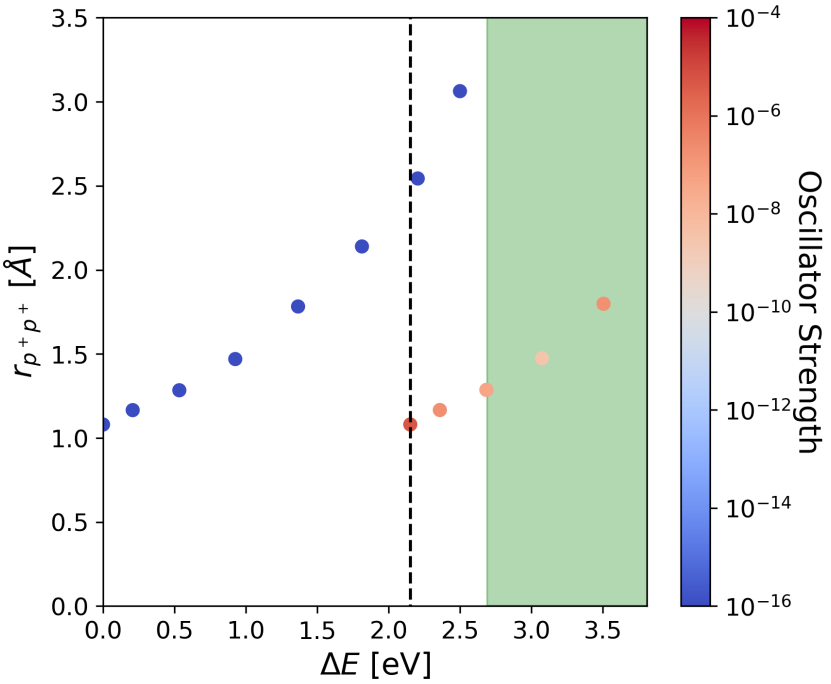

Figure S7: Quantized (i.e. bound) proton-proton distances for H_2^+ with respect to ground-state energy differences ΔE and corresponding oscillator strength in the *infinite proton mass limit*. The blue dots correspond to dressed bare matter states whereas red dots indicate the emerging bright photon replicas, which are absent without a cavity. The cavity frequency is $\omega = 2.15$ eV (dashed vertical line) with $\lambda = 0.051$ and zero COM motion. The green area indicates energy ranges beyond the p^+-dissociation limit according to matter-only simulations.

References

(1) Hesse, M.; Baye, D. Lagrange-Mesh Calculations of Three-Body Atoms and Molecules. *J. Phys. B: At., Mol. Opt. Phys.* **1999**, *32*, 5605–5617.

(2) Jestädt, R. Non-relativistic Three-body Systems and Finite Mass Effects. M.Sc. thesis, Freie-Universität Berlin, 2012.

(3) Hesse, M.; Baye, D. Lagrange-Mesh Calculations of Excited States of Three-Body Atoms and Molecules. *J. Phys. B: At., Mol. Opt. Phys.* **2001**, *34*, 1425.

(4) Marek, A.; Blum, V.; Johanni, R.; Havu, V.; Lang, B.; Auckenthaler, T.; Heinecke, A.;

Bungartz, H.-J.; Lederer, H. The ELPA Library: Scalable Parallel Eigenvalue Solutions for Electronic Structure Theory and Computational Science. *J. Phys. Condens. Matter* **2014**, *26*, 213201.

(5) Alexander, S.; Monkhorst, H. High-Accuracy Calculation of Muonic Molecules Using Random-Tempered Basis Sets. *Phys. Rev. A* **1988**, *38*, 26.

(6) Tancogne-Dejean, N.; Oliveira, M. J.; Andrade, X.; Appel, H.; Borca, C. H.; Le Breton, G.; Buchholz, F.; Castro, A.; Corni, S.; Correa, A. A. et al. Octopus, a Computational Framework for Exploring Light-Driven Phenomena and Quantum Dynamics in Extended and Finite Systems. *J. Chem. Phys.* **2020**, *152*, 124119.

(7) Flick, J.; Narang, P. Cavity-correlated Electron-Nuclear Dynamics from First Principles. *Phys. Rev. Lett.* **2018**, *121*, 113002.

(8) Korobov, V. I. Leading-Order Relativistic and Radiative Corrections to the Rovibrational Spectrum of H2+ and HD+ Molecular Ions. *Phys. Rev. A* **2006**, *74*, 052506.

(9) Flick, J.; Schäfer, C.; Ruggenthaler, M.; Appel, H.; Rubio, A. Ab Initio Optimized Effective Potentials for Real Molecules in Optical Cavities: Photon Contributions to the Molecular Ground State. *ACS Photonics* **2018**, *5*, 992–1005.